Vibration Analysis of Bidirectional Functionally Graded Porous Plates Using MITC3+

Nhan Thinh Hoang[1*], Thuan N.-T. Ho[2], Quoc Hoa Pham[3], Tran The Van[4]

[1]*Center of Innovation and Incubation (NIIC), Nguyen Tat Thanh University, Ho Chi Minh City, Vietnam; Email: htnhan@ntt.edu.vn*

[2]*Faculty of Civil Engineering, Ho Chi Minh City Open University, Ho Chi Minh City, Vietnam*

[3]*Tran Dai Nghia University, Ho Chi Minh City, Vietnam*

[4]*Faculty of Mechanical Engineering, Industrial University of Ho Chi Minh City, Ho Chi Minh City, Vietnam*

Abstracts: The article presents the vibration behavior of bidirectional functionally graded (BDFG) porous plates using the new triangular 3-node element (a cubic bubble function for the interpolation of the rotations to enrich the bending displacements) which is called the MITC3+ element. The BDFG porous plates have material properties varying in two directions with even and uneven porosity distribution. Based on Hamilton's principle, the motion equations for BDFG plates are derived. Then, some examples are performed to verify the accuracy and reliability of the proposed method. Finally, the new numerical results on the free vibration response of BDFG porous plates are provided.

Keywords: BDFG Plates; Free Vibration; FEM; MITC3+.

1. INTRODUCTION

Functionally graded materials (FGMs) represent an innovative category of composite materials, characterized by a continuous variation in material properties to achieve a predetermined composition profile. These materials are composed of two isotropic constituents, typically metals and ceramics, resulting in a heterogeneous structure. Over the past two decades, functionally graded material plates or panels have garnered significant attention from researchers due to their exceptional performance characteristics. They exhibit a desirable combination of high heat resistance, thanks to the presence of ceramics, and substantial mechanical strength and toughness derived from metals. Unlike conventional composite materials, FGMs exhibit a smooth and continuous variation in properties across adjacent layers. This unique feature enables the spatial optimization of microstructures to achieve optimal thermal and mechanical behavior tailored to specific applications. As a result, FGMs have found numerous applications across various engineering fields, including nuclear structures, biomedical engineering, electrical engineering, aircraft engineering, and nano FGMs. Additionally, they have gained considerable industrial significance. The following literature review provides valuable background information for the present research, further expanding upon the subject.

Houari Hachemi et al. [1] have introduced an innovative approach involving a high-order shear and normal deformation theory for analyzing the bending behavior of FGMs. In their study, they propose a novel method to determine the position of the neutral surface and derive the corresponding equilibrium equations based on this neutral surface. Dastjerdi et al. [2] have presented an innovative and unique quasi three-dimensional methodology for analyzing the bending behavior of moderately thick FG plates. Notably, the FGM plates considered in their study feature porosities that can be distributed in two forms: even and uneven distributions. An investigation is conducted on the bending behavior of thick rectangular plates made of porous functionally graded (FG) materials by Merdaci and Belghoul [3]. The analysis is based on a high-order shear deformation theory that considers both shear strain and normal deformation, eliminating the requirement for a shear correction factor. The equilibrium equations for the porous FG plates are derived, taking into account the specific characteristics of these materials.

In advanced aerospace crafts and shuttles are exposed to super-high temperatures, that having variation in two or more directions. So, these applications demanding new advanced materials which withstand at high temperature effectively. Multi-directional FGMs can be a good option to fulfill the demand of these applications. An investigation is conducted on the static bending, free vibration, and buckling analysis of porous BDFG plates using a combination of the first-order shear deformation theory (FSDT) and isogeometric analysis by Li et al. [4]. The BDFG plates considered in this study exhibit bi-directional gradients along both the thickness (z-axis) and x-axis directions, following a power law distribution. The porosity distributions are classified into two types: even and uneven. An investigation of dynamic behaviors of a sandwich plate containing an imperfect two dimensional functionally graded (2D-FG) core surrounded by two faces on a two-parameter elastic foundation and subjected to a moving load is carried out by Esmaeilzadeh et al. [5]. The fundamental equations are governed within the framework of first-order-shear deformation theory by utilizing Hamilton's principle, von-Karman geometrical nonlinearity and the principal of mixtures. Newmark direct integration procedure is implemented to transform the dynamic equations into a static form and then the kinetic dynamic relaxation numerical technique in conjunction with the finite difference discretization method are employed to solve the nonlinear partial differential governing equations. The eigenfrequency characteristics of a doubly-curved FG panel taking into account the influence of multi-directional grading and geometric large deformation are investigated by Ramteke et al. [6]. The study explores various material grading patterns and porosity distributions to model the FG structure. To establish a mathematical model, the researchers employ a mid-plane kinematics approach based on Higher-order Shear Deformation Theory (HSDT) and incorporate nonlinear strain terms using the Green-Lagrange formulation.

From the literature review, it is observed that very less work has been carried out on the analysis of BDFG plates using the finite element method and so far, there is no literature available for vibration analysis of BDFG plates using MITC3+. Hence in the present paper, an attempt has been made to develop a MITC3+ based on FSDT to investigate the vibration behaviour of BDFG plates. It is assumed that the material properties of FGM are changed gradually along the thickness of the plate from a ceramic-rich surface to a metal-rich surface. A detailed parametric study will be performed to examine the effects of thickness to small radius ratio, power-law indexes, and porosity volume fraction on the vibration characteristics of BDFG plates.

2. MATHEMATICAL FORMULATION

2.1. The Porous Bidirectional Functionally Material

The current study examines two types of porosity distribution in a BDFG plate with the dimensions of the length a, the width b and thickness h as illustrated in Figure 1. To calculate the effectiveness of Young's modulus E, Poisson's ratio υ, and mass density ρ of the BDFG plate, the rule of mixtures is utilized, as shown in the following formula:

$$\begin{aligned} E(x,z) &= E_c V_c(x,z) + E_m V_m(x,z), \\ \nu(x,z) &= \nu_c V_c(x,z) + \nu_m V_m(x,z), \\ \rho(x,z) &= \rho_c V_c(x,z) + \rho_m V_m(x,z) \end{aligned} \tag{1}$$

The volume fraction of the ceramic and metal phases, denoted by c and m respectively. The volumes displaced by the ceramic component and metal component are V_c and V_m, respectively, which can be computed as follows:

$$V_c(x,z) = \left(\frac{1}{2} + \frac{z}{h}\right)^n \left(\frac{x}{a}\right)^p, \qquad V_m(x,z) = 1 - V_c(x,z) \tag{2}$$

The power-law index of the material gradient through the thickness and x-axis directions is denoted by n and p, respectively. In the case where $n = 0$ and $p = 0$, the BDFG plate displays homogeneity and isotropy akin to a ceramic plate. Conversely, as both n and p approach the value ∞, the BDFG plate exhibits homogeneity and isotropy like that of a metal plate. When $n \neq 0$ and $p = 0$, the BDFG plate assumes the characteristics of a standard FG plate, whereas when only $p \neq 0$ and $n = 0$, it becomes a uniaxial FG plate.

The FG porous plates are made through several techniques, such as powder metallurgy, spray pyrolysis, and spark plasma sintering. The advantages of FG porous plates include improved mechanical properties such as increased toughness, enhanced energy absorption, and reduced weight compared to nonporous plates. However, the presence of porosity in the BDFG plates can lead to a reduction in its mechanical properties, such as Young's modulus E, Poisson's ratio ν, and mass density ρ. In the current study, two types of porosity are being investigated, namely, even distribution and uneven distribution. These two distribution types are mathematically represented by the following formulas as follows:

For even porosity type:

$$\begin{aligned} E(x,z) &= E_m + (E_c - E_m)V_c - \frac{\xi}{2}(E_c + E_m) \\ \nu(x,z) &= \nu_m + (\nu_c - \nu_m)V_c - \frac{\xi}{2}(\nu_c + \nu_m) \\ \rho(x,z) &= \rho_m + (\rho_c - \rho_m)V_c - \frac{\xi}{2}(\rho_c + \rho_m) \end{aligned} \tag{3}$$

For uneven porosity type:

$$\begin{aligned} E(x,z) &= E_m + (E_c - E_m)V_c - \frac{\xi}{2}\left(1 - \frac{2|z|}{h}\right)(E_c + E_m) \\ \nu(x,z) &= \nu_m + (\nu_c - \nu_m)V_c - \frac{\xi}{2}\left(1 - \frac{2|z|}{h}\right)(\nu_c + \nu_m) \\ \rho(x,z) &= \rho_m + (\rho_c - \rho_m)V_c - \frac{\xi}{2}\left(1 - \frac{2|z|}{h}\right)(\rho_c + \rho_m) \end{aligned} \tag{4}$$

where the symbol ξ represent the evaluation coefficient of the porosity volume of the plates.

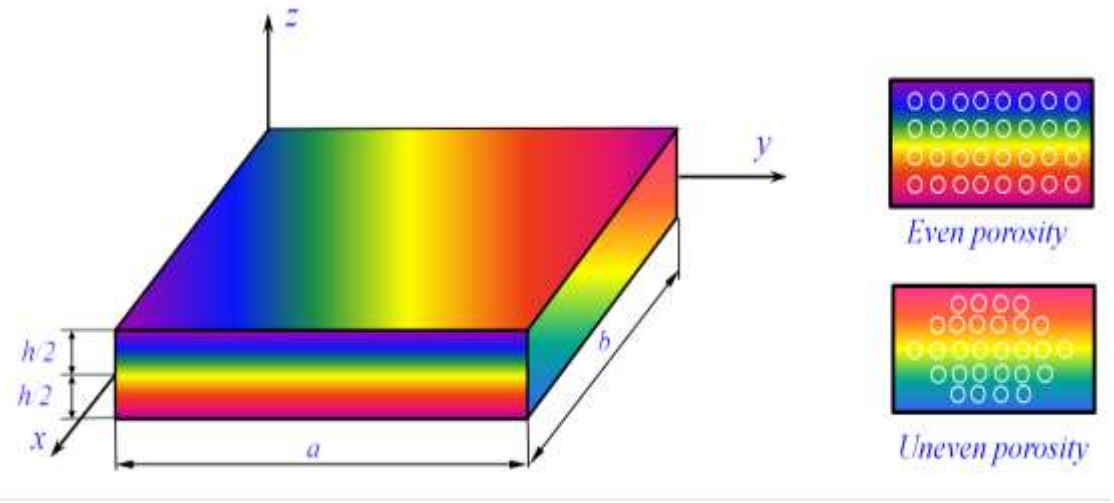

Figure 1. A porous bidirectional functionally graded plate model

2.2. Governing Equation For Improved First Order Shear Deformation Theory

Using the first order shear deformation theory (FSDT), a plate element's displacement field in the local coordinate system $Oxyz$ can be expressed as:

$$\begin{cases} u(x,y,z) = u_0(x,y) + z\beta_x(x,y), \\ v(x,y,z) = v_0(x,y) + z\beta_y(x,y), \\ w(x,y,z) = w_0(x,y) \end{cases} \tag{5}$$

here in u_0, v_0 and w_0 represent the displacements of the middle surface in the x, y and z directions, respectively; β_x and β_y denote the rotations in the xz and yz plane, respectively, as depicted in .

The strain components can be calculated from the displacement field as follows:

$$\boldsymbol{\varepsilon} = \begin{Bmatrix} \varepsilon_{xx} \\ \varepsilon_{yy} \\ \gamma_{xy} \end{Bmatrix} = \underbrace{\begin{Bmatrix} u_{0,x} \\ v_{0,y} \\ u_{0,y} + v_{0,x} \end{Bmatrix}}_{\boldsymbol{\varepsilon}_m} + z \underbrace{\begin{Bmatrix} \beta_{x,x} \\ \beta_{y,y} \\ \beta_{x,y} + \beta_{y,x} \end{Bmatrix}}_{\boldsymbol{\kappa}}, \tag{6}$$

$$\boldsymbol{\gamma} = \begin{Bmatrix} \gamma_{xz} \\ \gamma_{yz} \end{Bmatrix} = \begin{Bmatrix} w_{0,x} + \beta_x \\ w_{0,y} + \beta_y \end{Bmatrix}. \tag{7}$$

The linear stress-strain relation of porous BDFG plates, in accordance with Hooke's law, can be described as follows:

$$\begin{Bmatrix}\sigma_{xx}\\ \sigma_{yy}\\ \tau_{xy}\\ \tau_{xz}\\ \tau_{yz}\end{Bmatrix}=\begin{bmatrix}Q_{11} & Q_{12} & 0 & 0 & 0\\ Q_{21} & Q_{22} & 0 & 0 & 0\\ 0 & 0 & Q_{66} & 0 & 0\\ 0 & 0 & 0 & Q_{55} & 0\\ 0 & 0 & 0 & 0 & Q_{44}\end{bmatrix}\begin{Bmatrix}\varepsilon_{xx}\\ \varepsilon_{yy}\\ \gamma_{xy}\\ \gamma_{xz}\\ \gamma_{yz}\end{Bmatrix} \tag{8}$$

where

$$Q_{11}=Q_{22}=\frac{E(z)}{1-\upsilon(z)^2},\ Q_{12}=Q_{21}=\frac{\upsilon(z)E(z)}{1-\upsilon(z)^2},$$
$$Q_{44}=Q_{55}=Q_{66}=\frac{E(z)}{2(1+\upsilon(z))}. \tag{9}$$

It is well known that a constant shear correction coefficient, k=5/6, is commonly used for the shear stresses because of the FSDT theory's foundation on the hypothesis of linear shear strain distribution throughout the thickness

$$\begin{Bmatrix}\tau_{xz}\\ \tau_{yz}\end{Bmatrix}=k\begin{bmatrix}Q_{55} & 0\\ 0 & Q_{44}\end{bmatrix}\begin{Bmatrix}\gamma_{xz}\\ \gamma_{yz}\end{Bmatrix} \tag{10}$$

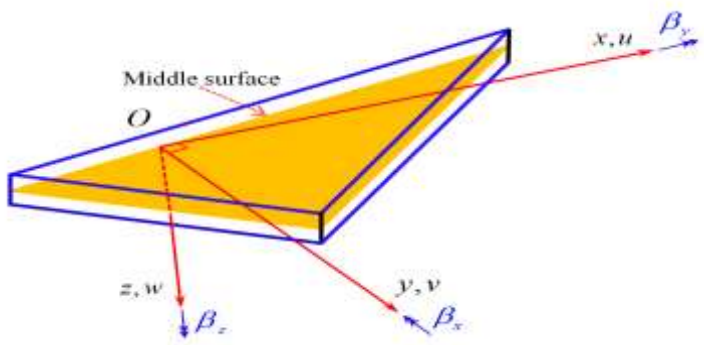

Figure 2. The triangular element

2.3. The Motion Equations Of BDFG Porous Plates

The governing equation of BDFG porous plates is derived using Hamilton's principle:

$$\int_0^T(\delta U+\delta W-\delta T)dt=0 \tag{11}$$

where δU, δW and δT are the variations of strain energy, potential energy and kinetic energy, respectively. The variation of strain energy is expressed by:

$$\delta \mathcal{U} = \frac{1}{2}\int_{\Omega} (\delta \boldsymbol{\varepsilon} \boldsymbol{D} \boldsymbol{\varepsilon}^T + \delta \boldsymbol{\gamma}^T \boldsymbol{D}_s \boldsymbol{\gamma}) \mathrm{d}\Omega \tag{12}$$

in which

$$\boldsymbol{\varepsilon} = \begin{bmatrix} \boldsymbol{\varepsilon}_m & \boldsymbol{\kappa} \end{bmatrix} \; ; \; \boldsymbol{D} = \begin{bmatrix} \boldsymbol{A} & \boldsymbol{B} \\ \boldsymbol{B} & \boldsymbol{C} \end{bmatrix} \tag{13}$$

with $\boldsymbol{A}$, $\boldsymbol{B}$, $\boldsymbol{C}$, and $\boldsymbol{D}_s$ are calculated by

$$(\boldsymbol{A}, \boldsymbol{B}, \boldsymbol{C}) = \int_{-h/2}^{h/2} (1, z, z^2) \begin{bmatrix} Q_{11} & Q_{12} & 0 \\ Q_{21} & Q_{22} & 0 \\ 0 & 0 & Q_{66} \end{bmatrix} \mathrm{d}z \tag{14}$$

$$\boldsymbol{D}_s = \int_{-h/2}^{h/2} 5/6 \begin{bmatrix} Q_{55} & 0 \\ 0 & Q_{44} \end{bmatrix} \mathrm{d}z \tag{15}$$

The variations of kinetic energy is:

$$\delta \mathcal{K} = \frac{1}{2}\int_{\Omega} \delta \dot{\boldsymbol{u}}^T \boldsymbol{m} \dot{\boldsymbol{u}} \mathrm{d}\Omega \tag{16}$$

in which $\boldsymbol{u}^T = [u_0 \quad v_0 \quad w_0 \quad \beta_x \quad \beta_y]$, and $\boldsymbol{m}$ is the mass matrix defined by

$$\boldsymbol{m} = \begin{bmatrix} m_1 & 0 & 0 & m_2 & 0 \\ & m_1 & 0 & 0 & m_2 \\ & & m_1 & 0 & 0 \\ & & & m_3 & 0 \\ sym & & & & m_3 \end{bmatrix} \tag{17}$$

with $(m_1, m_2, m_3) = \int_{-h/2}^{h/2} \rho(z)\,(1, z, z^2)\mathrm{d}z$ and $\rho(z)$ is mass density.

The variations of work done by applied forces is:

$$\delta W = \int_{\Omega} q \delta \boldsymbol{w}^T \mathrm{d}\Omega \tag{18}$$

q is the transverse load per unit area.

Substituting Eqs. (12), (16) and (18) into Eq. (11) the weak form for analysis of BDFG porous plates can be expressed by

$$\int_{\Omega} \delta\boldsymbol{\varepsilon}^T \boldsymbol{D}\boldsymbol{\varepsilon}\mathrm{d}\Omega + \int_{\Omega} \delta\boldsymbol{\gamma}^T \boldsymbol{D}_s\boldsymbol{\gamma}\mathrm{d}\Omega + \int_{\Omega} q\delta\boldsymbol{w}^T \mathrm{d}\Omega = \int_{\Omega} \ddot{\boldsymbol{u}}^T \boldsymbol{m}\ddot{\boldsymbol{u}}\mathrm{d}\Omega \tag{19}$$

2.4. Finite element procedure using MITC3+

The nodal displacement vector are represented using a triangular MITC3+ with five degrees of freedom for each node as follows **Error! Reference source not found.**:

$$\boldsymbol{d}_e = [\boldsymbol{d}_1^T \quad \boldsymbol{d}_2^T \quad \boldsymbol{d}_3^T \quad \boldsymbol{d}_4^T]^T \tag{20}$$

in which the node displacement is defined by

$$\boldsymbol{d}_i = \{u_{0i} \quad v_{0i} \quad w_i \quad \beta_{xi} \quad \beta_{yi}\} \text{ with } (i = 1 \div 4) \tag{21}$$

where the displacement components are interpolated by Lagrange function as follows **Error! Reference source not found.**:

$$\begin{gathered} u_0 = \sum_{i=1}^{4} N_i u_{0i};\ v_0 = \sum_{i=1}^{4} N_i v_{0i};\ w_0 = \sum_{i=1}^{4} N_i w_{0i}; \\ \theta_x = \sum_{i=1}^{4} N_i \theta_{xi};\ \theta_y = \sum_{i=1}^{4} N_i \theta_{yi} \end{gathered} \tag{22}$$

N_i is the shape function in the natural coordinate system (ξ, η) which is determined corresponding to the nodes at the vertices of the triangle ($i = 1, 2, 3$) and the bubble node ($i = 4$) located at the element's center as follows:

$$\begin{gathered} N_1 = 1 - \xi - \eta - 9\xi\eta(1 - \xi - \eta);\ N_2 = \xi - 9\xi\eta(1 - \xi - \eta); \\ N_3 = \eta - 9\xi\eta(1 - \xi - \eta);\ N_4 = 27\xi\eta(1 - \xi - \eta). \end{gathered} \tag{23}$$

Substituting Eq. (23) into Eqs. (6) and (7) the strain vectors can be expressed as follows:

$$\boldsymbol{\varepsilon}_m = \begin{Bmatrix} u_{0,x} \\ v_{0,y} \\ u_{0,y} + v_{0,x} \end{Bmatrix} = \sum_{i=1}^{4} \underbrace{\begin{bmatrix} N_{i,x} & 0 & 0 & 0 & 0 \\ 0 & N_{i,y} & 0 & 0 & 0 \\ N_{i,y} & N_{i,x} & 0 & 0 & 0 \end{bmatrix}}_{\boldsymbol{B}_{mi}} \underbrace{\begin{Bmatrix} u_{0i} \\ v_{0i} \\ w_i \\ \beta_{xi} \\ \beta_{yi} \end{Bmatrix}}_{\boldsymbol{d}_i} = \sum_{i=1}^{4} \boldsymbol{B}_{mi}\, \boldsymbol{d}_i; \tag{24}$$

$$\boldsymbol{\kappa} = \begin{Bmatrix} \beta_{x,x} \\ \beta_{y,y} \\ \beta_{x,y} + \beta_{y,x} \end{Bmatrix} = \sum_{i=1}^{4} \underbrace{\begin{bmatrix} 0 & 0 & N_{i,x} & 0 & 0 \\ 0 & 0 & 0 & N_{i,y} & 0 \\ 0 & 0 & N_{i,y} & N_{i,x} & 0 \end{bmatrix}}_{\boldsymbol{B}_{bi}} \underbrace{\begin{Bmatrix} u_{0i} \\ v_{0i} \\ w_i \\ \beta_{xi} \\ \beta_{yi} \end{Bmatrix}}_{\boldsymbol{d}_i} = \sum_{i=1}^{4} \boldsymbol{B}_{bi}\, \boldsymbol{d}_i; \tag{25}$$

$$\boldsymbol{\gamma} = \sum_{i=1}^{4} \underbrace{\begin{bmatrix} 0 & 0 & N_{i,y} & 0 & N_i \\ 0 & 0 & N_{i,x} & N_i & 0 \end{bmatrix}}_{\boldsymbol{B}_{si}} \underbrace{\begin{Bmatrix} u_{0i} \\ v_{0i} \\ w_i \\ \beta_{xi} \\ \beta_{yi} \end{Bmatrix}}_{\boldsymbol{d}_i} = \sum_{i=1}^{4} \boldsymbol{B}_{si}\, \boldsymbol{d}_i. \tag{26}$$

When the plate is thinner, the analysis results become inaccurate due to the phenomenon of shear locking. To fully overcome this issue, the authors propose the use of MITC3+ interpolation techniques to re-approximate the shear strain field:

$$\tilde{\gamma}_{\xi\zeta} = \frac{2}{3}\left(\gamma_{\xi\zeta}(B) - \frac{1}{2}\gamma_{\eta\zeta}(B)\right) + \frac{1}{3}\left(\gamma_{\xi\zeta}(C) + \frac{1}{2}\gamma_{\eta\zeta}(C)\right) + \frac{1}{3}\tilde{r}(3\xi - 1) \tag{27}$$

$$\tilde{\gamma}_{\eta\zeta} = \frac{2}{3}\left(\gamma_{\xi\zeta}(A) - \frac{1}{2}\gamma_{\eta\zeta}(A)\right) + \frac{1}{3}\left(\gamma_{\xi\zeta}(C) + \frac{1}{2}\gamma_{\eta\zeta}(C)\right) - \frac{1}{3}\tilde{r}(3\eta - 1) \tag{28}$$

with $\tilde{r} = \gamma_{\xi\zeta}(F) - \gamma_{\xi\zeta}(D) - \gamma_{\eta\zeta}(F) + \gamma_{\eta\zeta}(E)$; and $\gamma_{\xi\zeta}(I)$, $\gamma_{\eta\zeta}(I)$ are the values of the out-of-plane shear strain at the typing points *I* = *A, B, C, D, E, F* as shown in Table 1

Table 1 Coordinates of typing points of the MITC3+ element with d = 1/10000

Typing points	ζ	η	Typing points	ζ	η
A	1/6	2/3	D	1/3+d	1/3-2d
B	2/3	1/6	E	1/3-2d	1/3+d
C	1/6	2/6	F	1/3+d	1/3+d

Using the formula for transforming the shear strain of the out plane from the (x, y) coordinate system to the natural coordinate system (ξ, η) and substituting the shear strain approximation in the formulas, we can establish the relationship between the shear strain and the displacement field on the basis of MITC3+ technique is as follows:

$$\boldsymbol{\gamma} = \sum_{i=1}^{4} \boldsymbol{B}_{si}^{MITC3+}\, \boldsymbol{d}_i. \tag{29}$$

Replacing Eqs. (24), (25) and (29) into Eq. (19) , the motion equation of the plate element is:

$$\boldsymbol{K}_e\boldsymbol{d}_e + \boldsymbol{M}_e\ddot{\boldsymbol{d}}_e = \boldsymbol{F}_e \tag{30}$$

The element stiffness matrix $\boldsymbol{K}_e$ is:

$$\boldsymbol{K}_e = \int_{\Omega} \left(\begin{Bmatrix} \boldsymbol{B}_m \\ \boldsymbol{B}_b \\ \boldsymbol{B}_s \end{Bmatrix}^T \begin{bmatrix} \boldsymbol{A} & \boldsymbol{B} & 0 \\ \boldsymbol{B} & \boldsymbol{C} & 0 \\ 0 & 0 & \boldsymbol{D}_s \end{bmatrix} \begin{Bmatrix} \boldsymbol{B}_m \\ \boldsymbol{B}_b \\ \boldsymbol{B}_s \end{Bmatrix} \right) d\Omega \tag{31}$$

The element mass matrix $\boldsymbol{M}_e$ is:

$$\boldsymbol{M}_e = \int_{\psi} \boldsymbol{N}^T \boldsymbol{m} \boldsymbol{N}\, d\psi \tag{32}$$

where $\boldsymbol{N}$ is the shape function matrix determined by

$$\boldsymbol{N} = \sum_{i=1}^{4} \begin{bmatrix} N_i & 0 & 0 & 0 & 0 \\ & N_i & 0 & 0 & 0 \\ & & N_i & 0 & 0 \\ & & & N_i & 0 \\ sym & & & & N_i \end{bmatrix} \tag{33}$$

The element load vector $\boldsymbol{F}_e$ is:

$$\boldsymbol{F}_e = \int_{\Omega} \boldsymbol{N} \begin{bmatrix} 0 & 0 & q & 0 & 0 \end{bmatrix}^T d\Omega \tag{34}$$

where q is uniform distribution load.

Now, the motion equation of the BDFG porous plate is:

$$\boldsymbol{M}\ddot{\boldsymbol{q}} + \boldsymbol{K}\boldsymbol{d} = \boldsymbol{F} \tag{35}$$

where, $\boldsymbol{K} = \sum_{nel} \boldsymbol{K}_e$ is the global stiffness matrix, $\boldsymbol{M} = \sum_{nel} \boldsymbol{M}_e$ is the global mass matrix, and $\boldsymbol{F} = \sum_{nel} \boldsymbol{F}_e$ is the global load vector, all of which are obtained by summing up the corresponding element matrices and vectors over the total number of discretized elements denoted by "*nel*".

For the static bending analysis:

$$\boldsymbol{K}\boldsymbol{d} = \boldsymbol{F} \tag{36}$$

For the vibration analysis, the displacements can be expressed as $\boldsymbol{d} = \boldsymbol{q}e^{i\omega t}$, where $i^2 = -1$ and ω is the natural frequency. Therefore, Eq. (35) becomes:

$$(\boldsymbol{K} - \omega \boldsymbol{M})\boldsymbol{q} = \boldsymbol{0} \tag{37}$$

3. RESULTS AND DISCUSSIONS

In this study, let us consider the simply supported nonporous FG plates has geometrical dimensions of the length $a = b = 1m$; a thickness of $h = 0.1m$ and material parameters (Al/Al_2O_3) with $E_m = 70\text{Gpa}$; $E_c = 380\text{Gpa}$, $\rho_m = 2700\text{kg}/m^3$, $\rho_c = 3800\text{kg}/m^3$, v=0.3. The present study's results are compared with previously published works such as Demirhan and Taskin **Error! Reference source not found.** and Rezaei et al. **Error! Reference source not found.**, which used the analytical method based on the theory of four variables, presented in Table 2 and

Table **3**. The plates are discrete mesh 16x16. By observing the numerical outcomes in both tables, it is evident that the present work's results closely match those of the existing studies. The proposed formula in this study is thus deemed reliable and serves as the basis for examining the free vibration problems of the next bidirectional porous FG plate.

Table 2. Comparison the dimensionless natural frequency results of the FG porous plate with the change in thickness to length ratio and power index (Enven porosity distribution) $\Omega_1 = \Omega h\sqrt{\frac{\rho_m}{E_m}}$

a/h	*e*	Method	*p*			
			0	0.1	0.5	1
5	0	**Error! Reference source not found.**	0.43624	0.42035	0.37112	0.33425
		Error! Reference source not found.	0.41821	0.40322	0.35705	0.32249
		Present	0.4187	0.4039	0.3582	0.3232
	0.2	**Error! Reference source not found.**	0.44993	0.43150	0.36981	0.31684
		Error! Reference source not found.	0.43133	0.41396	0.35629	0.30681
		Present	0.4319	0.4147	0.3577	0.3082
	0.4	**Error! Reference source not found.**	0.46998	0.44808	0.36558	0.27482
		Error! Reference source not found.	0.45055	0.42994	0.35310	0.26825
		Present	0.4511	0.4307	0.3555	0.2735
10	0	**Error! Reference source not found.**	0.11514	0.11082	0.09763	0.08796
		Error! Reference source not found.	0.11369	0.10945	0.09651	0.08702

		Present	0.1144	0.1101	0.0972	0.0876
	0.2	**Error! Reference source not found.**	0.11875	0.11373	0.09719	0.08324
		Error! Reference source not found.	0.11726	0.11233	0.09612	0.08244
		Present	0.1180	0.1130	0.0968	0.0831
	0.4	**Error! Reference source not found.**	0.12405	0.11807	0.09592	0.07194
		Error! Reference source not found.	0.12249	0.11662	0.09494	0.07142
		Present	0.1233	0.1173	0.0958	0.0730
0 2	0	**Error! Reference source not found.**	0.02922	0.02811	0.02475	0.02230
		Error! Reference source not found.	0.02912	0.02802	0.02467	0.02224
		Present	0.0294	0.0282	0.0249	0.0224
	0.2	**Error! Reference source not found.**	0.03014	0.02885	0.02463	0.02110
		Error! Reference source not found.	0.03003	0.02875	0.02456	0.02104
		Present	0.0303	0.0290	0.0248	0.0212
	0.4	**Error! Reference source not found.**	0.03148	0.02995	0.02429	0.01821
		Error! Reference source not found.	0.03137	0.02985	0.02423	0.01817
		Present	0.0316	0.0301	0.0245	0.0186

Table 3. Comparison the dimensionless natural frequency results of the FG porous plate with the change in thickness to length ratio and power index (Unenven porosity distribution) $\Omega_1 = \Omega h \sqrt{\frac{\rho_m}{E_m}}$

a/h	*e*	Method	*p*			
			0	0.1	0.5	1
5	0	**Error! Reference source not found.**	0.43624	0.42035	0.37112	0.33425
		Error! Reference source not found.	0.41821	0.40322	0.35705	0.32249
		Present	0.4187	0.4039	0.3582	0.3232
	0.2	**Error! Reference source not found.**	0.44885	0.43141	0.37440	0.32764
		Error! Reference source	0.42933	0.41367	0.36404	0.32496

		not found.				
		Present	0.4292	0.4138	0.3664	0.3307
	0.4	**Error! Reference source not found.**	0.46522	0.44589	0.37814	0.33460
		Error! Reference source not found.	0.44227	0.42589	0.37215	0.32709
		Present	0.4413	0.4253	0.3764	0.3410
10	0	**Error! Reference source not found.**	0.11514	0.11082	0.09763	0.08796
		Error! Reference source not found.	0.11369	0.10945	0.09651	0.08702
		Present	0.1144	0.1101	0.0972	0.0876
	0.2	**Error! Reference source not found.**	0.11862	0.11388	0.10013	0.08859
		Error! Reference source not found.	0.11699	0.11256	0.09864	0.08789
		Present	0.1177	0.1132	0.0999	0.0902
	0.4	**Error! Reference source not found.**	0.12314	0.11787	0.10216	0.08991
		Error! Reference source not found.	0.12085	0.11621	0.10112	0.08868
		Present	0.1215	0.1169	0.1031	0.0938
20	0	**Error! Reference source not found.**	0.02922	0.02812	0.02476	0.02230
		Error! Reference source not found.	0.02912	0.02802	0.02467	0.02224
		Present	0.0294	0.0282	0.0249	0.0224
	0.2	**Error! Reference source not found.**	0.03013	0.02891	0.02542	0.02271
		Error! Reference source not found.	0.02999	0.02884	0.02524	0.02247
		Present	0.0302	0.0291	0.0256	0.0231
	0.4	**Error! Reference source not found.**	0.03129	0.02993	0.02606	0.02288
		Error! Reference source not found.	0.03101	0.02980	0.02590	0.02269

		Present	0.0313	0.0300	0.0265	0.0241

Table 4 and Table 5 present the dimensionless natural frequency of the simply supported porous BDFG plate, which varies based on parameters such as length and thickness ratio, power law index, and pore factor. As we observe from the tables, when the values of n and p increase, the dimensionless natural frequency decreases, which is reasonable because it leads to an increase in the proportion of metal in the material of the plate, thus decreasing the plate's stiffness and natural frequency. The natural frequency is at its lowest when n and p reach the maximum value. Furthermore, the porosity coefficient has a significant impact on the frequency of the porous BDFG plates, as an increase in the porosity coefficient causes the natural frequency to decrease. Additionally, the thickness of the plate has a considerable effect on its frequency.

Table 4. Dimensionless natural frequency of the BDFG porous plate with the change in thickness to length ratio and power index (Enven porosity distribution) $\Omega_1 = \Omega h \sqrt{\frac{\rho_m}{E_m}}$

a/h	e	n	p			
			0	0.1	0.5	1
5	0	0	0.4187	0.4074	0.3680	0.3325
		0.1	0.4039	0.3931	0.3559	0.3228
		0.5	0.3582	0.3495	0.3203	0.2953
		1	0.3232	0.3165	0.2947	0.2761
	0.1	0	0.4247	0.4126	0.3690	0.3278
		0.1	0.4088	0.3972	0.3557	0.3170
		0.5	0.3581	0.3484	0.3151	0.2854
		1	0.3170	0.3095	0.2844	0.2624
	0.2	0	0.4319	0.4188	0.3698	0.3196
		0.1	0.4147	0.4020	0.3550	0.3075
		0.5	0.3577	0.3469	0.3078	0.2704
		1	0.3082	0.2996	0.2694	0.2415
10	0	0	0.1144	0.1114	0.1010	0.0914
		0.1	0.1101	0.1072	0.0974	0.0885
		0.5	0.0972	0.0949	0.0872	0.0806
		1	0.0876	0.0859	0.0802	0.0753
	0.1	0	0.1161	0.1128	0.1014	0.0903
		0.1	0.1114	0.1083	0.0974	0.0871
		0.5	0.0971	0.0945	0.0858	0.0780
		1	0.0858	0.0838	0.0773	0.0716
	0.2	0	0.1180	0.1145	0.1017	0.0886
		0.1	0.1130	0.1096	0.0974	0.0849
		0.5	0.0968	0.0940	0.0838	0.0741
		1	0.0831	0.0809	0.0731	0.0659
20	0	0	0.0294	0.0286	0.0259	0.0235
		0.1	0.0282	0.0275	0.0250	0.0227
		0.5	0.0249	0.0243	0.0224	0.0207

		1	0.0224	0.0220	0.0206	0.0193
	0.1	0	0.0298	0.0290	0.0260	0.0232
		0.1	0.0286	0.0278	0.0250	0.0224
		0.5	0.0248	0.0242	0.0220	0.0200
		1	0.0219	0.0214	0.0198	0.0184
	0.2	0	0.0303	0.0294	0.0262	0.0228
		0.1	0.0290	0.0281	0.0250	0.0219
		0.5	0.0248	0.0240	0.0215	0.0190
		1	0.0212	0.0207	0.0187	0.0169

Table 5. Dimensionless natural frequency of the BDFG porous plate with the change in thickness to length ratio and power index (Unenven porosity distribution)

a/h	e	n	p			
			0	0.1	0.5	1
5	0	0	0.4187	0.4074	0.3680	0.3325
		0.1	0.4039	0.3931	0.3559	0.3228
		0.5	0.3582	0.3495	0.3203	0.2953
		1	0.3232	0.3165	0.2947	0.2761
	0.1	0	0.4238	0.4122	0.3713	0.3338
		0.1	0.4087	0.3976	0.3588	0.3239
		0.5	0.3621	0.3531	0.3224	0.2957
		1	0.3267	0.3197	0.2964	0.2762
	0.2	0	0.4292	0.4173	0.3746	0.3346
		0.1	0.4138	0.4024	0.3619	0.3244
		0.5	0.3664	0.3571	0.3247	0.2958
		1	0.3307	0.3234	0.2984	0.2762
10	0	0	0.1144	0.1114	0.1010	0.0914
		0.1	0.1101	0.1072	0.0974	0.0885
		0.5	0.0972	0.0949	0.0872	0.0806
		1	0.0876	0.0859	0.0802	0.0753
	0.1	0	0.1160	0.1129	0.1022	0.0922
		0.1	0.1116	0.1087	0.0985	0.0893
		0.5	0.0985	0.0961	0.0881	0.0811
		1	0.0888	0.0870	0.0810	0.0758
	0.2	0	0.1177	0.1145	0.1035	0.0930
		0.1	0.1132	0.1102	0.0997	0.0900
		0.5	0.0999	0.0974	0.0891	0.0817
		1	0.0902	0.0883	0.0820	0.0764
20	0	0	0.0294	0.0286	0.0259	0.0235
		0.1	0.0282	0.0275	0.0250	0.0227
		0.5	0.0249	0.0243	0.0224	0.0207
		1	0.0224	0.0220	0.0206	0.0193
	0.1	0	0.0298	0.0290	0.0263	0.0237

		0.1	0.0286	0.0279	0.0253	0.0230
		0.5	0.0252	0.0246	0.0226	0.0208
		1	0.0227	0.0223	0.0208	0.0195
	0.2	0	0.0302	0.0294	0.0266	0.0240
		0.1	0.0291	0.0283	0.0257	0.0232
		0.5	0.0256	0.0250	0.0229	0.0210
		1	0.0231	0.0227	0.0211	0.0197

CONCLUSIONS

In this work, the MITC3+ element are proposed to investigate the free vibrations of bidirectional functionally graded porous plates. The correctness of the current method was compared with reliable statements in the published literature. Based on an evaluation of the influence of various parameters on the vibration response of the BDFG porous plates, our findings can be summarized as follows:

- MITC3+ element applied for the first time to the calculation of three directional BDFG porous plates.
- The porosity coefficient has a significant impact on the frequency of the porous BDFG plates, as an increase in the porosity coefficient causes the natural frequency to decrease.
- The results of this study will be a benchmark for BDFG porous plate studies in the future.

REFERENCES

[1] Hachemi H., Bousahla A. A., Kaci A., Bourada F., Tounsi A., Benrahou K. H. & Mahmoud S. R. Bending analysis of functionally graded plates using a new refined quasi-3D shear deformation theory and the concept of the neutral surface position. Steel and Composite Structures, An International Journal, 39(1), (2021) 51-64.

[2] Dastjerdi S., Malikan M., Dimitri R., & Tornabene F. Nonlocal elasticity analysis of moderately thick porous functionally graded plates in a hygro-thermal environment. Composite Structures, 255, (2021) 112925.

[3] Merdaci S., & Belghoul H. High-order shear theory for static analysis of functionally graded plates with porosities. Comptes Rendus Mécanique, 347(3), (2019) 207-217.

[4] Li S., Zheng S., & Chen D. Porosity-dependent isogeometric analysis of bi-directional functionally graded plates. Thin-Walled Structures, 156, (2020) 106999.

[5] Esmaeilzadeh M., Golmakani M. E., Luo Y., & Bodaghi M. Transient behavior of imperfect bi-directional functionally graded sandwich plates under moving loads. Engineering with Computers, (2021) 1-11.

[6] Ramteke P. M., Panda S. K., & Patel B. Nonlinear eigenfrequency characteristics of multi-directional functionally graded porous panels. Composite Structures, 279, (2022) 114707.

[7] Jam, F. A., Singh, S. K. G., Ng, B., & Aziz, N. (2016). Interactive effects of Gender and Leadership Styles on Open Service Innovation: A Study of Malaysian Doctors, *International Journal of Economics Research*, 13(3), 1287-1304.

[8] Lee Youngyu, Phill-Seung Lee, and Klaus-Jürgen Bathe, The MITC3+ shell element and its performance." Computers & Structures 138 (2014) 12-23.

[9] Demirhan PA, Taskin V, Bending and free vibration analysis of Levy-type porous functionally graded plate using state space approach, Composites Part B, 2019

[10] Rezaei AS, Saidi AR, Abrishamdari M, Pour Mohammadi MH. Natural frequencies of functionally graded plates with porosities via a simple four variable plate theory: An analytical approach. Thin-Walled Structures (2017)

DOI: https://doi.org/10.15379/ijmst.v10i3.1696